Submitted to

International Europhysics Conference on High Energy Physics, EPS03, July 17-23, 2003, Aachen
(Abstract **088** Parallel Session **5**)

XXI International Symposium on Lepton and Photon Interactions, LP03, August 11-16, 2003, Fermilab

www-h1.desy.de/h1/www/publications/conf/conf_list.html

Measurement of the Diffractive Deep-Inelastic Scattering Cross Section at Low Q^2

H1 Collaboration

Abstract

A new measurement is presented of the diffractive deep-inelastic scattering process $ep \rightarrow eXY$, where Y is a proton or low mass excitation. The results are obtained from a data sample of 3.4 pb^{-1} taken by the H1 experiment at HERA, with unbiased triggers. The measurement is presented in the form of a 3-dimensional reduced cross section $\sigma_r^{D(3)}(\beta, Q^2, x_{I\!P})$ which is integrated over the region $M_Y < 1.6$ GeV and $|t| < 1$ GeV^2 and covers the kinematic range $1.5 \leq Q^2 \leq 12$ GeV^2, $0.01 \leq \beta \leq 0.9$ and $10^{-4} \lesssim x_{I\!P} < 0.03$. The results extend and improve the precision at the lowest Q^2 considerably compared to previous measurements. Interpreted through Regge-motivated fits to the $x_{I\!P}$ dependence, the data suggest a lower value of the effective pomeron intercept than that obtained from higher Q^2 data. The data are also compared with the predictions of a NLO DGLAP QCD fit to higher Q^2 data. In the perturbative region $Q^2 > 3$ GeV^2, the data confirm the dominance of a gluon distribution extending to large fractional momenta in the diffractive parton densities. A colour dipole model based on the exchange of pairs of gluons is also compared with the data.

1 Introduction

A new H1 measurement of the reduced diffractive cross section $\sigma_r^{D(3)}$ is presented where $\sigma_r^{D(3)}$ is related to the diffractive structure function $F_2^{D(3)}$ by

$$\sigma_r^{D(3)} = F_2^{D(3)} - \frac{y^2}{1+(1-y)^2} F_L^{D(3)} . \tag{1}$$

The manner in which $\sigma_r^{D(3)}$ is extracted is very similar to that presented in [1] (first reported in [2]), but the present analysis extends the kinematic range to lower values of Q^2. The measured region is of particular interest for the study of the transition from the high Q^2 regime where perturbative QCD techniques [3] are applicable [1, 4] to the non-perturbative photoproduction regime, where Regge phenomenology with a soft pomeron describes the data well [5, 6].

2 Diffractive Kinematics

Figure 1 shows the generic diffractive process $ep \rightarrow eXY$ which proceeds via a net colour singlet exchange. X is a hadronic system of mass M_X produced at the γ^* vertex and Y is a proton or low mass excitation of mass M_Y. The inclusive variables for DIS have the usual definitions,

$$Q^2 = -q^2, \quad y = \frac{P.q}{P.k}, \quad x = \frac{-q^2}{2P.q} , \tag{2}$$

where the four-momenta of the positron, proton and photon are given respectively by k, P and q. The four-momentum transfer at the proton vertex is given by,

$$t = (P - p_Y)^2 , \tag{3}$$

where p_Y is the four-momentum of the hadronic Y system. The diffractive variables,

$$x_{I\!P} = \frac{q.(P - p_Y)}{q.P}, \quad \beta = \frac{Q^2}{2q.(P - p_Y)} , \tag{4}$$

are defined, where in the infinite momentum frame of the proton $x_{I\!P}$ is the fraction of the four-momentum of the proton taken by the colourless exchange and β is the fraction of the four-momentum of the exchange carried by the struck parton. The measurement presented here is integrated over the region $M_Y < 1.6$ GeV and $|t| < 1$ GeV^2 as the system Y is not detected and these variables are not well measured.

3 Event Selection and Reconstruction

This measurement of the reduced diffractive cross section was performed using data taken during 1999 with the H1 detector at HERA [7]. During a dedicated run with unbiased triggers a

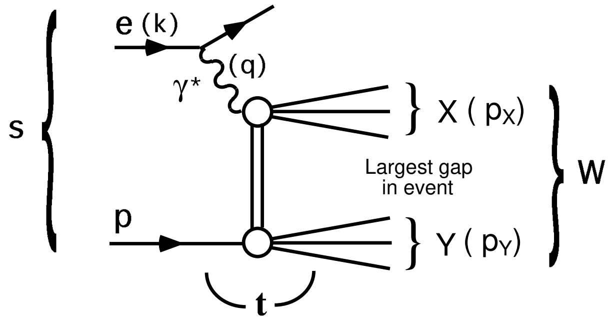

Figure 1: The generic diffractive process $ep \rightarrow eXY$ at HERA. The positron with four-momentum k couples to a photon (γ^*) which interacts with the proton via a colour singlet exchange to produce separate hadronic final state systems X and Y. These two systems are widely separated in rapidity if their masses are much smaller than W.

sample of e^+p data was collected which allowed access to low values of Q^2. The proton beam energy for this running period was 920 GeV, which differs from the analysis of 1997 data [1] where the beam energy was 820 GeV. The positron beam energy of 27.6 GeV was the same for both years.

The measurement with this data sample of 3.4 pb^{-1} is restricted to the region $1.25 < Q^2 < 13.5$ GeV^2, $y > 0.04$ and $x_{I\!P} < 0.03$. The basic event selection is very similar to the procedure adopted in [1] except that scattered positron candidates in the backward SPACAL calorimeter with energy $E'_e > 6$ GeV were selected. Several improvements have been made to the selection of diffractive events, which is based on an absence of activity in forward[1] detector components which are sensitive to energy flow close to the outgoing proton direction. The Forward Tagger System (FTS), a series of scintillators installed around the outgoing proton beampipe in 1998, was required to show no activity beyond noise thresholds. The same requirements were imposed for the Proton Remnant Tagger (PRT), further scintillator planes with improved efficiency compared with earlier running periods, as well as the Forward Muon Detector and the Plug calorimeter. The improved sensitivity to hadronic activity in the very forward direction compared with previous years allowed the cut on the pseudorapidity of the most forward energy deposit in the Liquid Argon Calorimeter to be relaxed to $\eta_{\max} < 3.3$.

For the reconstruction of Q^2, x and y, a combination of the electron and double angle methods was used, which optimises the experimental resolutions throughout the measured phase space [1,4]. Also as in previous H1 measurements, the mass of the hadronic final state X was reconstructed as

$$M_X^2 = (E^2 - p_x^2 - p_y^2 - p_z^2)_h \cdot \frac{y}{y_h} \, , \tag{5}$$

where y denotes the value reconstructed from the combined electron / double-angle method and y_h is reconstructed using only final state hadrons. A global factor of 1.07 is applied to the measured M_X to correct for residual losses. β and $x_{I\!P}$ are reconstructed as

$$\beta = \frac{Q^2}{Q^2 + M_X^2}, \quad x_{I\!P} = \frac{x}{\beta} \, . \tag{6}$$

[1] In the H1 coordinate system $\theta = 0°$ corresponds to the outgoing proton beam direction. The forward direction corresponds to small θ and positive rapidity.

4 Simulations

A combination of several Monte Carlo generators was used to model experimental resolutions and to determine efficiencies and acceptances. The inclusive and diffractive components of deep inelastic scattering were modelled separately using DJANGO [8], for $M_Y > 5$ GeV or $x_{I\!P} > 0.1$, and the 'saturation' colour dipole model [9] as implemented in RAPGAP [10] for the elastic process with $x_{I\!P} < 0.1$. The RAPGAP implementation of the saturation model was reweighted as a function of $x_{I\!P}$, β and y as it originally failed to provide a good description of the data. Additional contributions at large β arising from vector meson production were simulated using DIFFVM [11]. The photoproduction and QED-Compton backgrounds were modelled using the PHOJET [12] and COMPTON [13] Monte Carlo generators. Figure 2 shows control distributions for several important variables after applying the inclusive event selection, but not the diffractive (forward detector) requirements. DJANGO and PHOJET were used to model the distributions. A good description is obtained, illustrating excellent control over the inclusive DIS sample. Figure 3 shows control distributions for a selection of variables after the full diffractive cuts with contributions from all Monte Carlo models.

5 Reduced Diffractive Cross Section Extraction

The measured differential cross section is related to the reduced diffractive cross section by

$$\frac{\mathrm{d}^3\sigma_{ep\to eXY}}{\mathrm{d}x\,\mathrm{d}Q^2\,\mathrm{d}x_{I\!P}} = \frac{4\pi\alpha_{em}^2}{xQ^4}\ (1-y+\frac{y^2}{2})\ \sigma_r^{D(3)}(x,Q^2,x_{I\!P})\ , \tag{7}$$

where the systems X and Y are separated by the largest gap in the rapidity distribution of the final state hadrons. The reduced cross section is extracted with the requirements of acceptance of the diffractive selection greater than 50%, acceptance for the detection of the electron in the SPACAL calorimeter greater than 20% and bin purities in excess of 20%. The measurement is quoted at the Born level with initial and final state radiation and QED virtual loop corrections calculated using RAPGAP interfaced to HERACLES [14]. The improved forward detector selection results in a smaller correction for smearing about the measurement limits in M_Y and t than was the case in [1]. This correction is $0.5\pm5.4\%$, evaluated using the DIFFVM simulations of elastic and proton dissociative diffractive scattering.

The reduced diffractive cross sections presented in the next section are shown with full systematic errors arising from uncertainties in detector energy scales and efficiencies and from variations in the kinematic distributions of Monte Carlo models. A normalisation error of 5.9%, arising dominantly from the correction applied for migrations across the $M_Y = 1.6$ GeV, $|t| < 1$ GeV^2 measurement limit, is not shown.

6 Results

The quantity $x_{I\!P}\sigma_r^{D(3)}$ extracted from the 1999 data is presented in a binning scheme optimised to study the $x_{I\!P}$ dependence and its variation with β and Q^2 in figures 4 and 5. In figure 4, the data are compared with the higher Q^2 measurement in [1]. In the region of overlap ($6.5 \leq Q^2 \leq 12$ GeV^2), there is good agreement between the two datasets, especially considering that the present measurement has several modifications in the experimental technique (new forward detectors, different Monte Carlo models and different proton beam energy for example). The results from this analysis extend the measured kinematic region in $\sigma_r^{D(3)}$ to considerably lower Q^2 with high precision. In figure 5, the data are compared with another recent H1 measurement [15] in which diffractive events were selected on the basis of a leading proton tagged in the Forward Proton Spectrometer (FPS). The FPS data are scaled by a factor of 1.10 to match the small proton dissociation contribution with $M_Y < 1.6$ GeV in the present data. The two datasets, which have highly uncorrelated systematic effects, are in reasonable agreement. The present measurement has the better precision.

6.1 The $x_{I\!P}$ dependence of $\sigma_r^{D(3)}$

A phenomenological fit to the $x_{I\!P}$ dependence of $\sigma_r^{D(3)}(\beta, Q^2, x_{I\!P})$, following the method in [1, 4], was performed to the new data alone. The data were parameterised according to a Regge-motivated form with 'pomeron' and sub-leading 'meson' exchange contributions;

$$\sigma_r^{D(3)}(\beta, Q^2, x_{I\!P}) = f_{\mathrm{I\!P}}(x_{I\!P}) A_{\mathrm{I\!P}}(\beta, Q^2) + f_{\mathrm{I\!R}}(x_{I\!P}) A_{\mathrm{I\!R}}(\beta, Q^2) \; , \tag{8}$$

where

$$f_{\mathrm{I\!P},\mathrm{I\!R}}(x_{I\!P}) = \int_{-1}^{t_{min}} \frac{e^{B_{\mathrm{I\!P},\mathrm{I\!R}} t}}{x_{I\!P}^{2\alpha_{\mathrm{I\!P},\mathrm{I\!R}}(t)-1}} \mathrm{d}t \; . \tag{9}$$

Here, $|t_{min}|$ is the minimum value of $|t|$ allowed kinematically and the pomeron and meson trajectories are assumed to be linear ($\alpha_{\mathrm{I\!P},\mathrm{I\!R}}(t) = \alpha_{\mathrm{I\!P},\mathrm{I\!R}}(0) + \alpha'_{\mathrm{I\!P},\mathrm{I\!R}} t$). The values of parameters which were fixed in the fits, were taken from fixed target data (see [5]);

$$\begin{aligned}
\alpha_{\mathrm{I\!R}}(0) &= 0.50 \pm 0.16 \; , && (10)\\
\alpha'_{\mathrm{I\!P}} &= 0.26 \pm 0.26 \text{ GeV}^{-2} \; , && (11)\\
\alpha'_{\mathrm{I\!R}} &= 0.90 \pm 0.10 \text{ GeV}^{-2} \; , && (12)\\
B_{\mathrm{I\!P}} &= 4.6 \pm^{3.4}_{2.6} \text{ GeV}^{-2}, && (13)\\
B_{\mathrm{I\!R}} &= 2.0 \pm 2.0 \text{ GeV}^{-2}. && (14)
\end{aligned}$$

The value of $\alpha_{\mathrm{I\!P}}(0)$ was assumed to be constant for all β and Q^2 values fitted. The pomeron and meson normalisations $A_{\mathrm{I\!P}}(\beta, Q^2)$ and $A_{\mathrm{I\!R}}(\beta, Q^2)$ were left free in each (β, Q^2) bin. Data points with $y > 0.45$ were excluded from the fits in order to minimise the possible effects of the unmeasured $F_L^{D(3)}$ (taken to be zero by default). Bins in (β, Q^2) in which there are less than four data points were also excluded. The results of the fit are shown in figure 6. The fit reproduces the data well, and has a χ^2/ndf of $103.4/103$. Due to the y and $x_{I\!P}$ cuts, the meson contribution is poorly constrained, though there is a significant increase in the χ^2/ndf if the meson contribution is omitted. The apparently large meson component at high β is an artifact of the fitting procedure, resulting from the free normalisation of the pomeron and meson contributions in each bin, coupled with the relatively large statistical errors in this region.

The value of $\alpha_{I\!P}(0)$ resulting from the fit is

$$\alpha_{I\!P}(0) = 1.110 \pm 0.020(\text{stat.}) \pm 0.024(\text{syst.}) \pm^{0.068}_{0.033} (\text{model}) , \quad (15)$$

where the model dependence uncertainty arises from variations of the fixed parameters as given in equations 10-14 and from the variation $0 < F_L^D < F_2^D$. This latter uncertainty is the dominant source of error.

Figure 7 shows $\alpha_{I\!P}(0)$ from this measurement compared with previous H1 measurements [1, 4–6]. There is a suggestion of a dependence of $\alpha_{I\!P}(0)$ on Q^2, though firm conclusions are not possible with the present uncertainties. Figure 8 shows the 1997 [1] and 1999 H1 data with the uncertainty due to the F_L^D variation illustrated by the yellow band. Taking $F_L^D = 0$, the present result is consistent with the soft pomeron intercept $\alpha_{I\!P}(0) \sim 1.08$ [16], which describes soft hadron-hadron interactions. However, if F_L^D is closer to F_2^D, as might be expected from the large gluonic component of the diffractive parton densities [1, 4], the Q^2 dependence of $\alpha_{I\!P}(0)$ in diffractive dissociation is compatible with that from inclusive DIS data [17]. It is thus clear that constraints on F_L^D are urgently required in order to interpret the energy dependence of diffractive DIS. Such constraints have been obtained indirectly from next-to-leading order (NLO) QCD fits [1].

6.2 The β and Q^2 dependence of $\sigma_r^{D(3)}$

Figures 9, 10 and 11 show the β dependences of $x_{I\!P}\sigma_r^{D(3)}$ for fixed Q^2 and $x_{I\!P} = 0.001$, 0.003 and 0.01 respectively. The Q^2 dependences at fixed β are shown for the same $x_{I\!P}$ values in figures 12, 13 and 14 respectively. The 1999 low Q^2 data are compared with the 1997 results. Overall there is good agreement between the data sets in the region of overlap. Figures 15 and 16 provide a summary of the full $\sigma_r^{D(3)}$ data, without the $x_{I\!P}$ factor in this case, for all $x_{I\!P}$ bins.

Figures 9 - 11 show that the general trends of the β dependence observed in [1] continue to lower Q^2. The β dependence is relatively flat, and clearly rises towards the highest β values at low Q^2 (figure 9). The extended Q^2 range of the new data enhances the sensitivity to the scaling violations of $\sigma_r^{D(3)}$. The new data confirm that scaling violations with positive $\partial\sigma_r^{D(3)}/\partial \ln Q^2$ persist up to large values of β (figures 12 - 14). At the largest β values studied, the scaling violations clearly become negative (figure 12). The β and Q^2 dependences of the data can be understood in terms of the dominance of gluons with large momentum fractions in the diffractive exchange at low scales, evolving to lower momentum fractions with increasing Q^2.

In [1], NLO QCD fits were performed to the 1997 data in order to extract diffractive parton densities of the proton. The predictions from these fits are overlaid in figures 9- 14 in the region $Q^2 > 3.0$ GeV^2 (corresponding to the starting scale Q_0^2 for QCD evolution in the fit), $M_X > 2$ GeV (corresponding to the cut applied for data entering the fit) and $y < 0.6$ (in order to minimise the influence of F_L and hence the sensitivity to the different beam energies of the two datasets). The fits reproduce the new data at $Q^2 = 5$ GeV^2 well. For $Q^2 = 3.5$ GeV^2, there is an indication that the fits fall below the data, suggesting that improved parton densities could be obtained by including the new data in this region in the QCD fits.

In figure 17, the 1999 and 1997 data for $x_{I\!P} = 0.01$ are compared with the predictions of the colour dipole model of Golec-Biernat and Wüsthoff [9], in which diffractive DIS is modelled by the scattering of $q\bar{q}$ fluctuations of longitudinally polarised photons and $q\bar{q}$ and $q\bar{q}g$ fluctuations of transversely polarised photons from the proton via the exchange of pairs of gluons. Relative to the original predictions, an additional colour factor of $(4/9)^2$ has been included for the $q\bar{q}g$ contribution [18]. With this additional factor, the model undershoots the data in the low β region where the $q\bar{q}g$ term dominates, except at the lowest Q^2 values. Similar conclusions are reached for different values of $x_{I\!P}$ [1].

7 Summary

A sample of diffractive deep-inelastic scattering events corresponding to a luminosity of 3.4 pb^{-1} was selected from H1 data collected with minimally biased triggers in 1999. The reduced diffractive cross section $\sigma_r^{D(3)}(\beta, Q^2, x_{I\!P})$ was measured in the kinematic region covering $1.5 \leq Q^2 \leq 12$ GeV^2, $0.01 \leq \beta \leq 0.9$ and $10^{-4} \lesssim x_{I\!P} < 0.03$, providing an extension to lower Q^2 compared with previous H1 data. The new 1999 data represent the most precise H1 $\sigma_r^{D(3)}(\beta, Q^2, x_{I\!P})$ results for $Q^2 < 15$ GeV^2. The new data points agree with previous H1 results based on 1997 [1] data throughout the region of overlap in phase space, despite the existence of several differences in the measurement techniques.

From the $x_{I\!P}$ dependence of the data, a value is extracted for the effective pomeron intercept by performing a Regge motivated fit to the data. The extracted $\alpha_{I\!P}(0)$ is somewhat lower than that obtained in other H1 measurements at higher Q^2 [1,4], though firm conclusions are still not possible with the present uncertainties. The new binning scheme introduced in [1] allowed detailed examination of the β and Q^2 dependence of the data and a good agreement was observed with the recent measurement on 1997 data and with the QCD fits performed in [1]. The data thus confirm that the diffractive parton densities are dominated by a gluon density extending to large fractional momenta.

Acknowledgements

We are grateful to the HERA machine group whose outstanding efforts have made and continue to make this experiment possible. We thank the engineers and technicians for their work in constructing and now maintaining the H1 detector, our funding agencies for financial support, the DESY technical staff for continual assistance, and the DESY directorate for the hospitality which they extend to the non DESY members of the collaboration.

References

[1] H1 Collaboration, *Measurement and NLO DGLAP QCD Interpretation of Diffractive Deep-Inelastic Scattering at HERA*, paper 980 submitted to this conference.

[2] H1 Collaboration, *Measurement of the Diffractive Structure Function* $F_2^{D(3)}(\beta, Q^2, x_{I\!P})$ *at HERA*, paper 808 submitted to EPS2001, Budapest, Hungary, July 2001.

[3] J. Collins, Phys. Rev. D57 (1998) 3051 and erratum-ibid. D61 (2000) 019902.

[4] H1 Collaboration, C. Adloff et al., Z. Phys. C76 (1997) 613.

[5] H1 Collaboration, C. Adloff et al., Z. Phys. C74 (1997) 221.

[6] H1 Collaboration, *Diffractive Dissociation in Photoproduction at HERA*, paper 985 submitted to this conference.

[7] H1 Collaboration, I. Abt et al., Nucl. Instr. Meth. A386 (1997) 310 and 348.

[8] G. Schuler, H. Spiesberger, Proc. of the Workshop on Physics at HERA, Vol. 3, eds. W. Buchmüller, G. Ingelman, Hamburg, DESY (1992) 1419.

[9] K. Golec-Biernat, M. Wüsthoff, Phys. Rev. D59 (1999) 014017;
K. Golec-Biernat, M. Wüsthoff, Phys. Rev. D60 (1999) 114023;
J. Bartels, K. Golec-Biernat, H. Kowalski, Phys. Rev. D66 (2002) 014001.

[10] H. Jung, Comp. Phys. Commun. 86 (1995) 147.

[11] B. List, A. Mastroberardino, *DIFFVM: A Monte Carlo Generator for diffractive processes in ep scattering*, in A. Doyle, G. Grindhammer, G. Ingelman, H. Jung (eds.): *Monte Carlo Generators for HERA Physics*, DESY-PROC-1999-02 (1999) 396.

[12] R. Engel, J. Ranft, Phys. Rev. D54 (1996) 4244.

[13] A. Courou, P. Kessler, Phys. Rev. D46 (1992) 117.

[14] A. Kwiatkowski, H, Speisberger, H. Möhring, Comp. Phys. Comm. 69 (1992) 155.

[15] H1 Collaboration, *Measurement of Semi-inclusive Diffractive Deep-Inelastic Scattering with a Leading Proton at HERA*, paper 984 submitted to this conference;
paper 809 submitted to EPS2001, Budapest, Hungary, July 2001.

[16] A. Donnachie, P. Landshoff, Phys. Lett. B296 (1992) 227;
J. Cudell, K. Kang, S. Kim, Phys. Lett. B395 (1997) 311.

[17] H1 Collaboration, C. Adloff et al., Phys. Lett. B520 (2001) 183.

[18] K. Golec-Biernat, private communication.

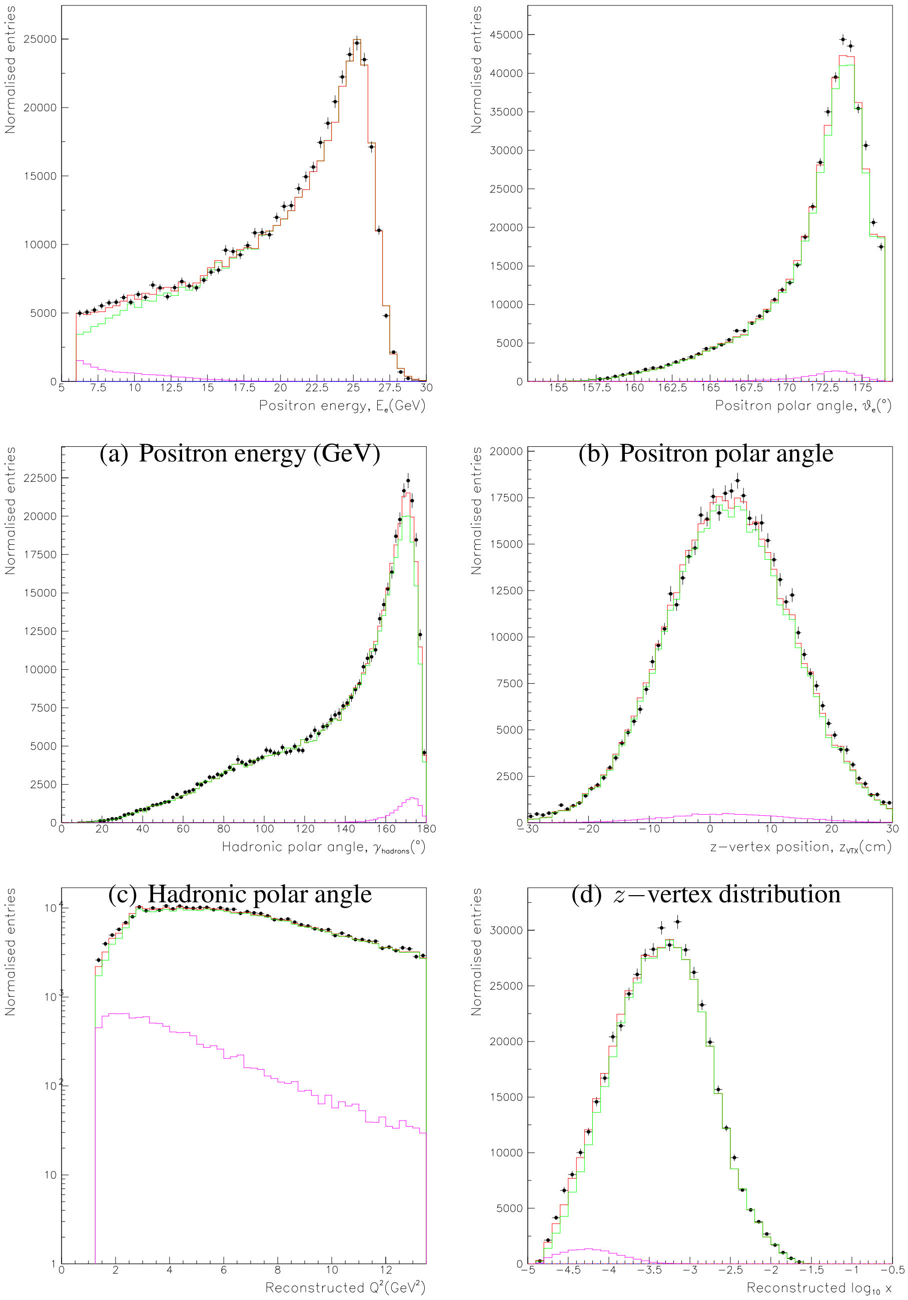

(a) Positron energy (GeV)

(b) Positron polar angle

(c) Hadronic polar angle

(d) $z-$vertex distribution

(e) Photon virtuality Q^2 (GeV^2)

(f) $\log x$

Figure 2: Control distributions before the application of the forward detector selection. The data points are shown, with statistical errors, by the black points. The DJANGO and PHOJET Monte Carlo contributions are denoted by the green and purple histograms respectively and the total Monte Carlo simulation is shown in red.

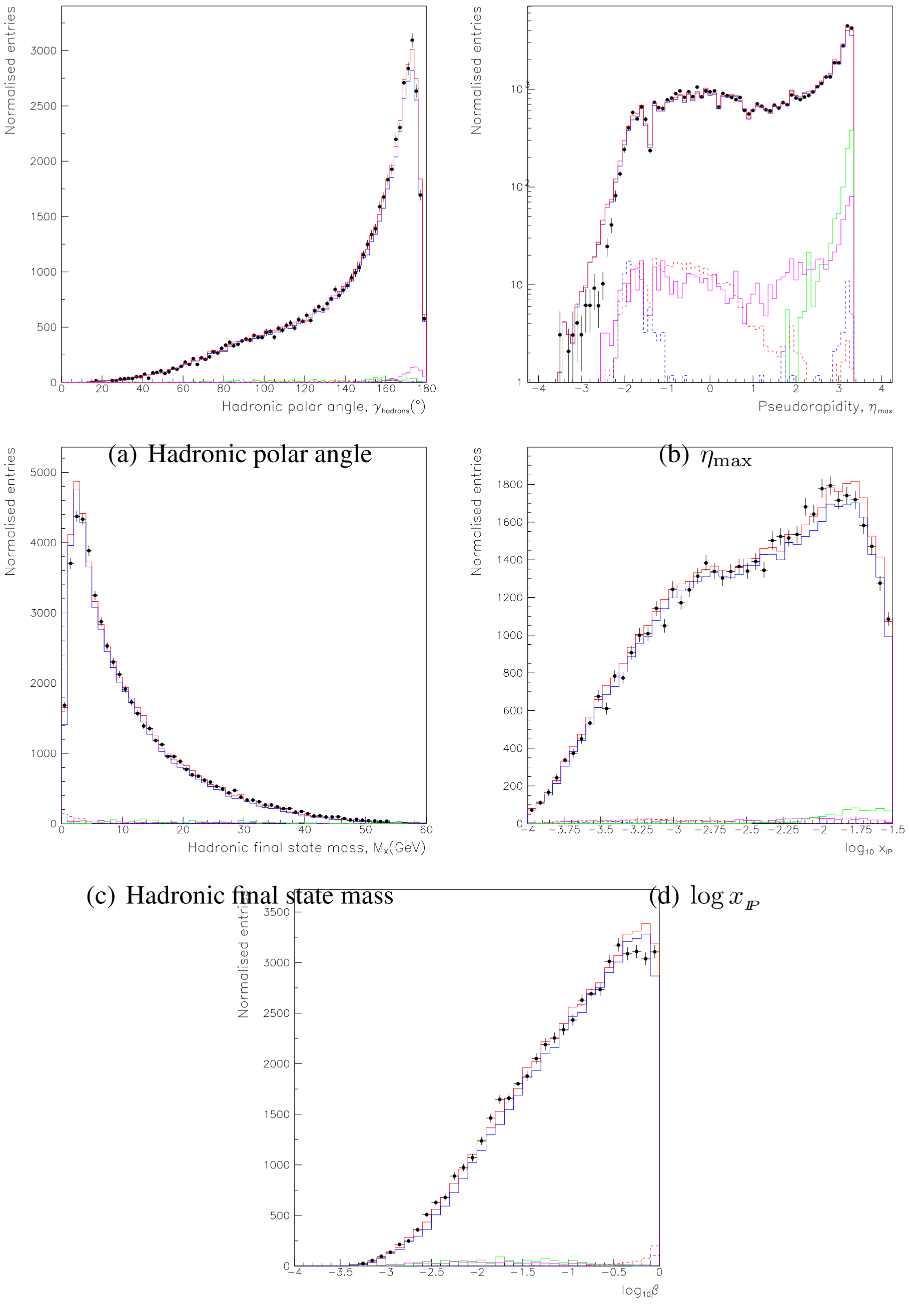

(a) Hadronic polar angle

(b) $\eta_{\max}$

(c) Hadronic final state mass

(d) $\log x_{I\!P}$

(e) $\log \beta$

Figure 3: Control distributions after the application of the full diffractive selection. The data points are shown, with statistical errors, by the black points. The DJANGO and PHOJET Monte Carlo contributions are denoted by the green and purple histograms and the RAPGAP, DIFFVM and COMPTON contributions are represented by the blue, dotted red and dotted blue histograms respectively. The total Monte Carlo simulation is shown in red.

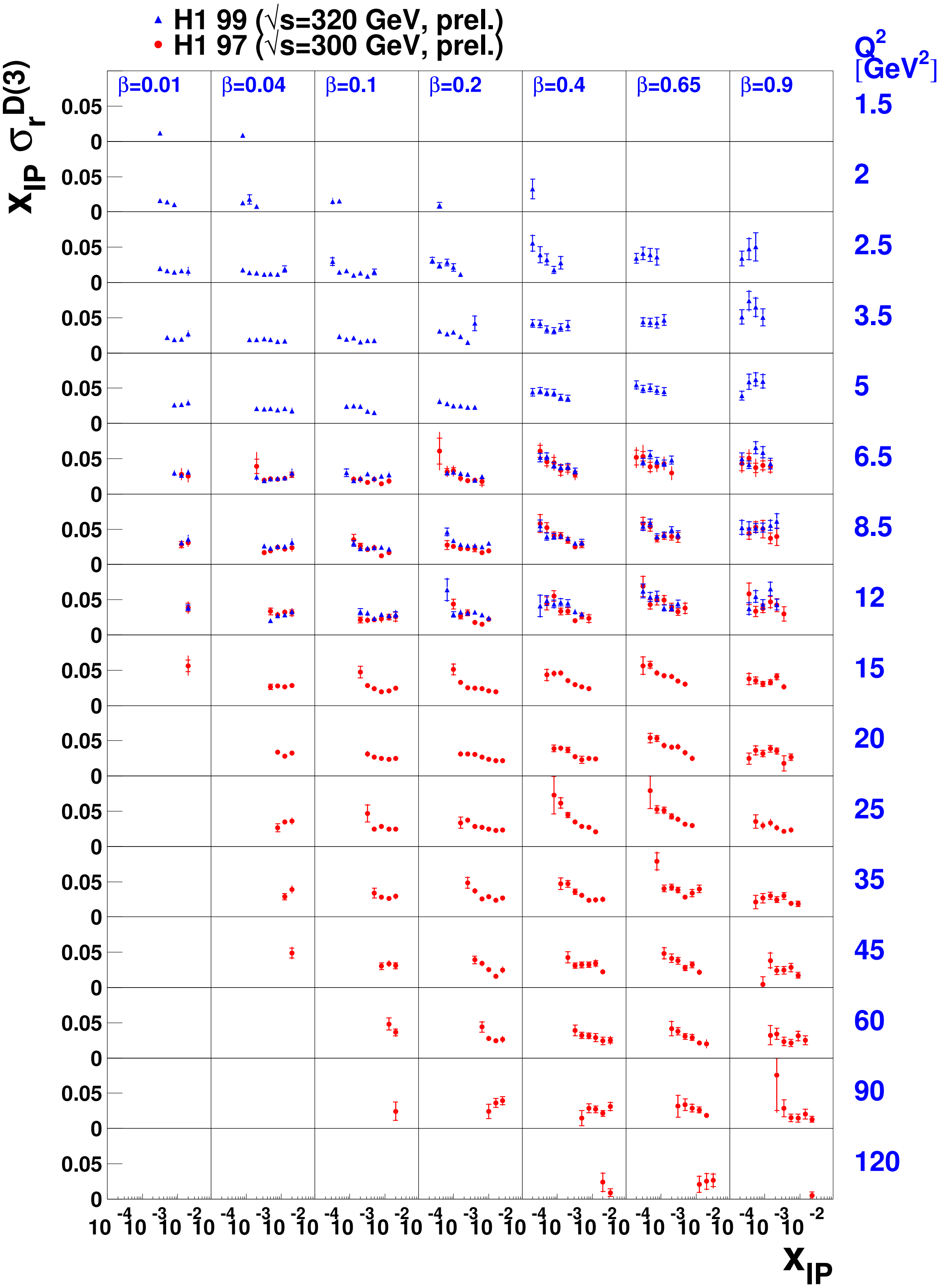

Figure 4: The reduced diffractive cross section from this measurement (blue triangles) compared with a recent H1 measurement [1] at larger Q^2 (red filled circles). $x_{I\!P}\sigma_r^{D(3)}(\beta, Q^2, x_{I\!P})$ is shown as a function of $x_{I\!P}$ for fixed values of β and Q^2. Both measurements are shown with inner statistical and outer total (statistical and systematic added in quadrature) errors. Normalisation uncertainties of 5.9% for the present data and 6.7% for [1] are not shown.

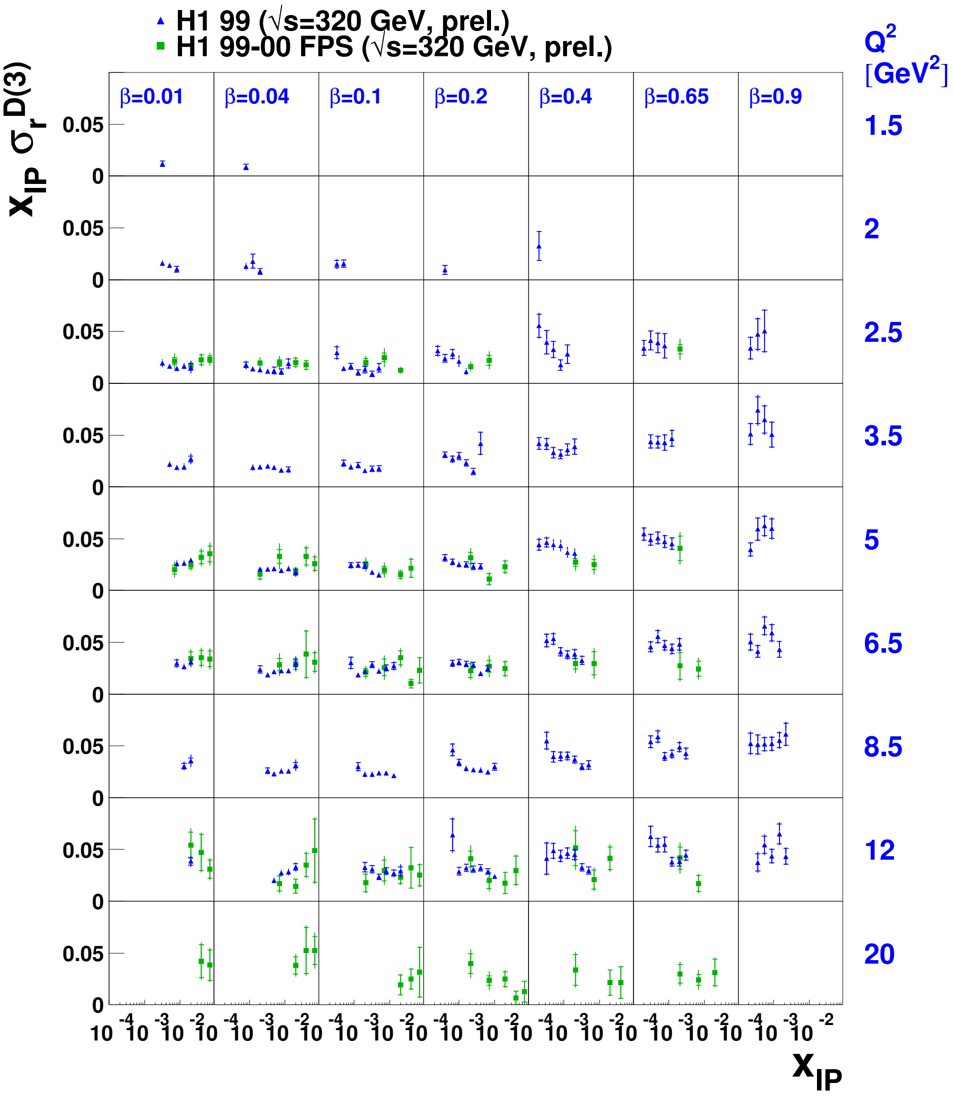

Figure 5: The reduced diffractive cross section from this measurement (blue triangles) compared with a recent H1 measurement [15] in which diffractive events were selected by direct tagging of leading protons (green squares). $x_{I\!P}\sigma_r^{D(3)}(\beta, Q^2, x_{I\!P})$ is shown as a function of $x_{I\!P}$ for fixed values of β and Q^2. Both measurements are shown with inner statistical and outer total (statistical and systematic added in quadrature) errors. A normalisation uncertainty of 5.9% for the present data is not shown.

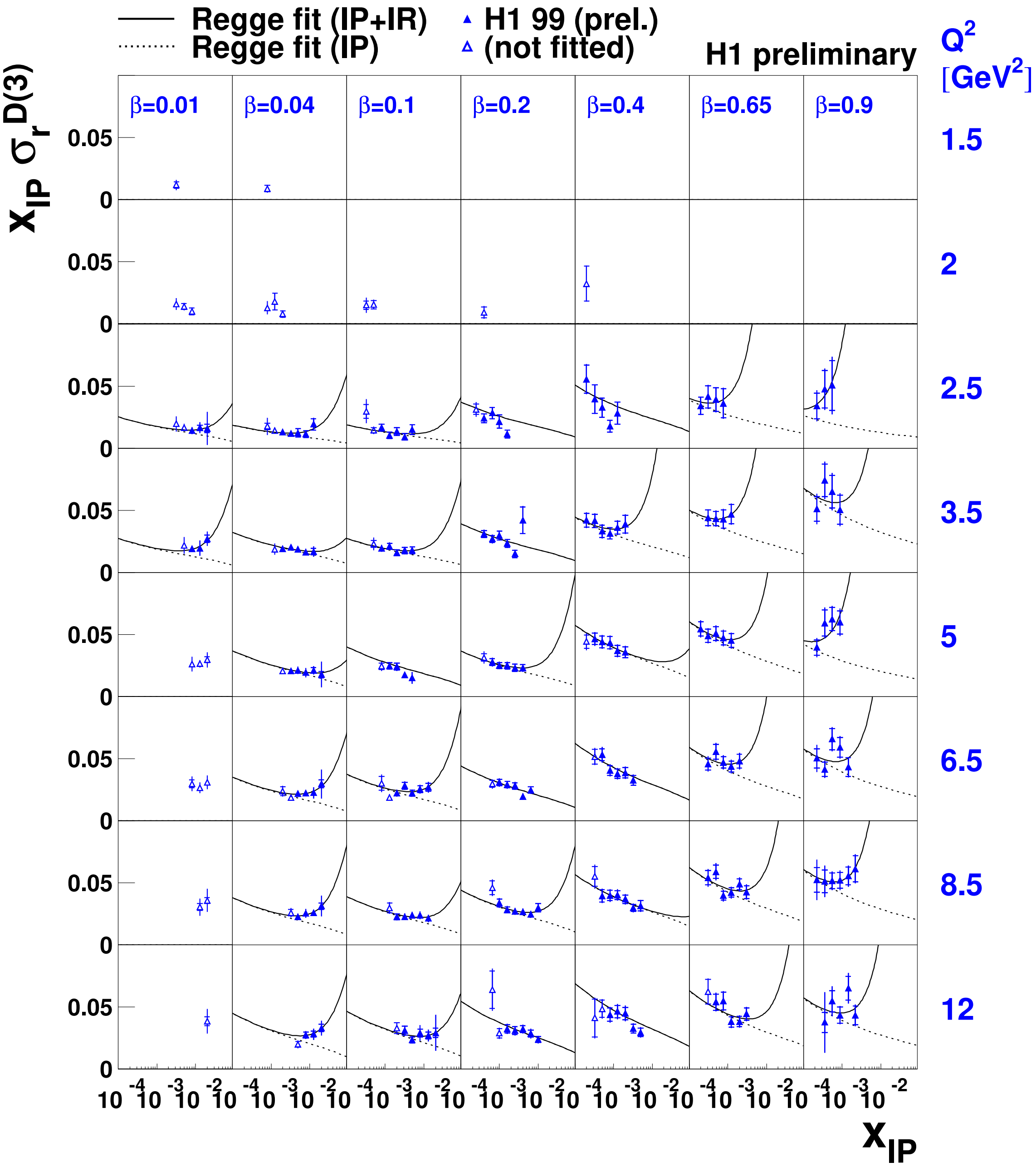

Figure 6: The reduced diffractive cross section extracted from the 1999 data. $x_{I\!P}\sigma_r^{D(3)}(\beta, Q^2, x_{I\!P})$ is shown as a function of $x_{I\!P}$ for fixed values of β and Q^2, with β increasing from left to right and Q^2 increasing from top to bottom. The result of a phenomenological Regge fit to the data is also shown for combined pomeron and meson exchange contributions (solid curve) and pomeron exchange only (dotted curve). The open symbols indicate data points which were excluded from the fit.

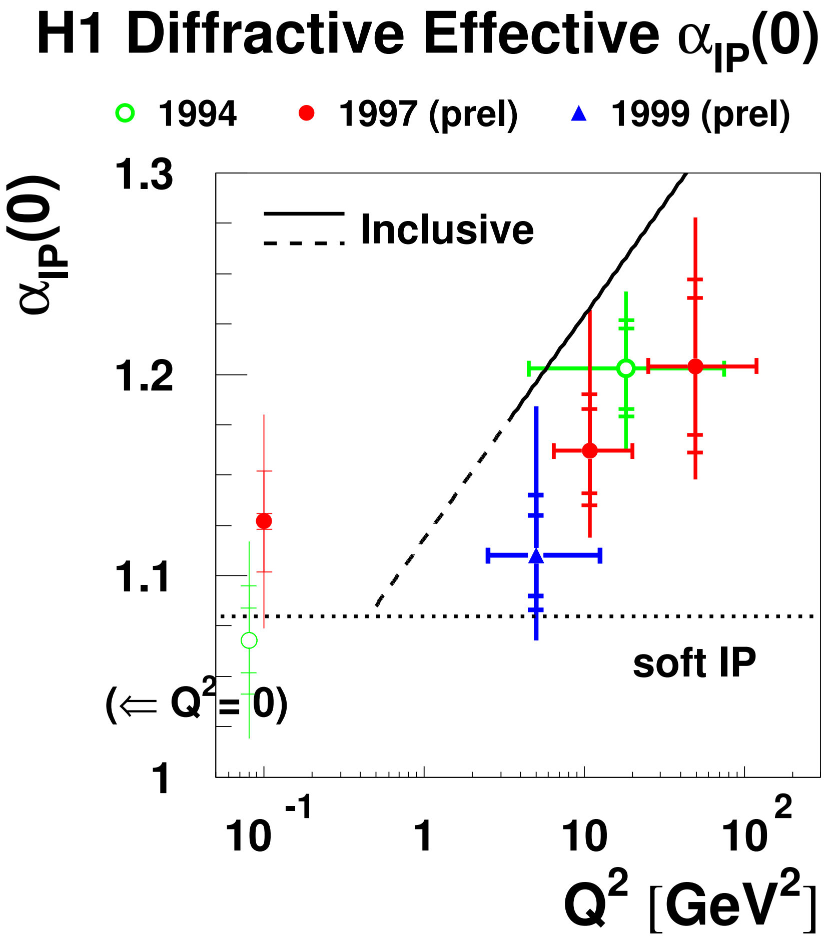

Figure 7: The effective pomeron intercept $\alpha_{\mathbb{P}}(0)$ shown as a function of Q^2 for H1 diffractive data. The blue triangle is the value extracted in this analysis, the red filled circles are the values from the 1997 data [1, 6] and the green open circles represent measurements from 1994 data [4, 5]. The inner error bars represent statistical errors and the middle error bars include systematic errors added in quadrature. The outer error bars represent total errors, including those arising from model dependences. The solid line represents $\alpha_{\mathbb{P}}(0) = 1 + \lambda$ from a parameterisation of the form $F_2 = cx^{-\lambda(Q^2)}$ to inclusive $F_2(x, Q^2)$ H1 data [17] for $x < 0.01$. The dashed line represents the extension of this parameterisation to lower Q^2 values than those included in the original fit.

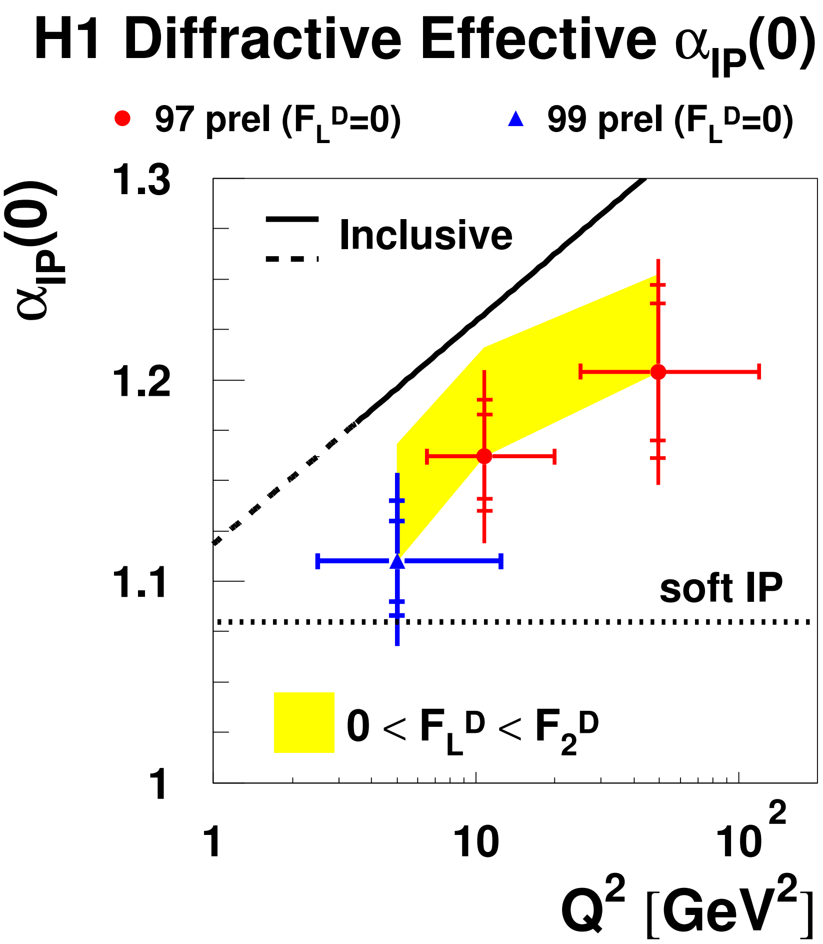

Figure 8: The effective pomeron intercept $\alpha_{\mathbb{P}}(0)$ shown as a function of Q^2 for H1 diffractive DIS data. The blue triangle is the value extracted in this analysis and the red filled circles are the values from the 1997 data [1]. The inner error bars represent statistical errors and the middle error bars include systematic errors added in quadrature. The outer error bars include in addition the model dependence errors with the exception of that arising from the variation of F_L^D. The yellow band represents the effect of varying the assumptions on F_L^D from $F_L^D = 0$ (taken by default) to $F_L^D = F_2^D$. The solid line represents $\alpha_{\mathbb{P}}(0) = 1 + \lambda$ from a parameterisation of the form $F_2 = cx^{-\lambda(Q^2)}$ to inclusive $F_2(x, Q^2)$ H1 data [17] for $x < 0.01$. The dashed line represents the extension of this parameterisation to lower Q^2 values than those included in the original fit.

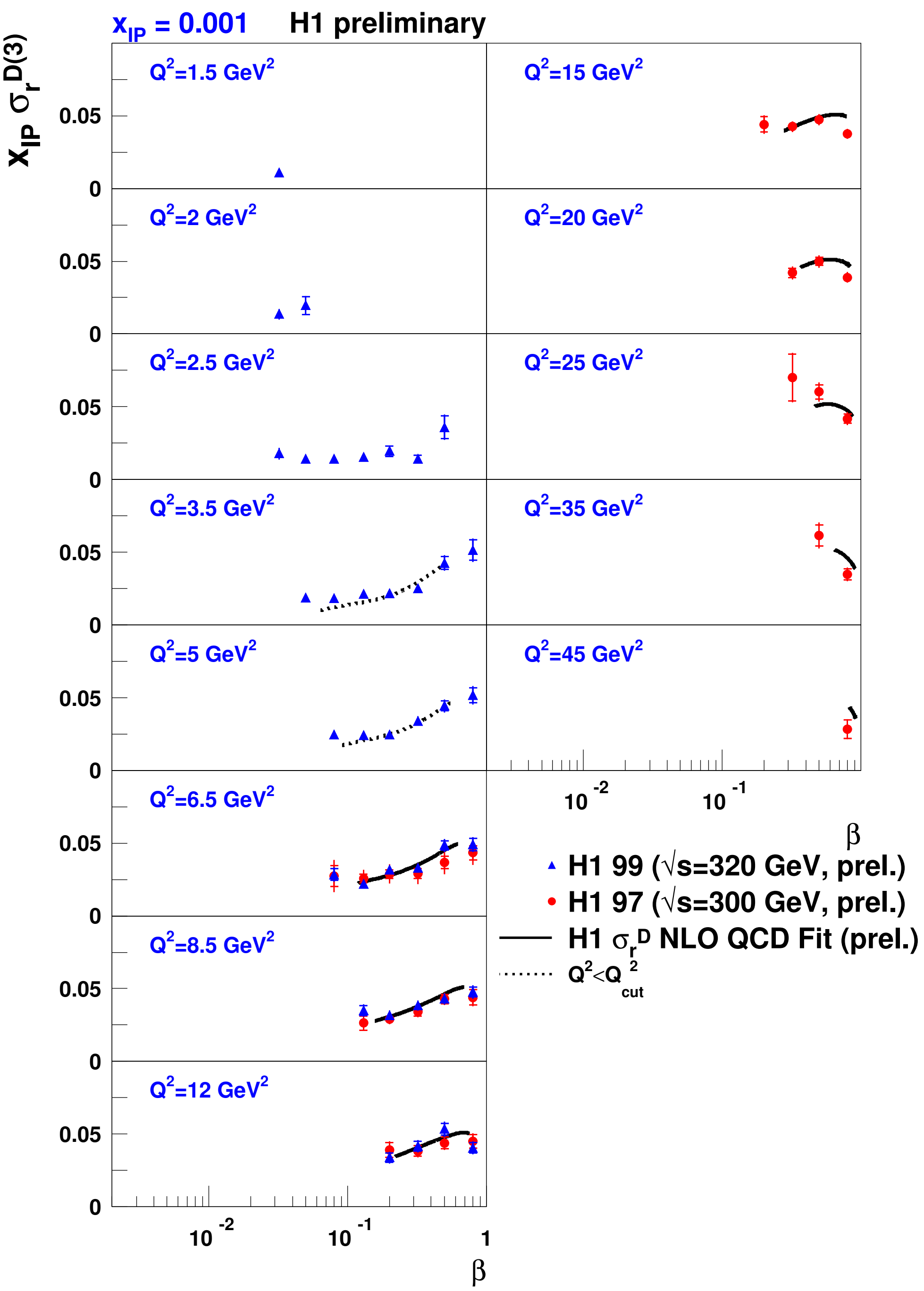

Figure 9: The reduced diffractive cross section $x_{\mathbb{P}}\sigma_r^{D(3)}(\beta, Q^2, x_{\mathbb{P}})$ (blue triangles) compared with a recent H1 measurement [1] (red circles). $x_{\mathbb{P}}\sigma_r^{D(3)}(\beta, Q^2, x_{\mathbb{P}})$ is shown as a function of β at $x_{\mathbb{P}} = 0.001$ for fixed values of Q^2. The prediction for $x_{\mathbb{P}}\sigma_r^{D(3)}$ for $\sqrt{s} = 300$ GeV from the NLO DGLAP QCD fit in [1] is shown with the solid line for $Q^2 \geq 6.5$ GeV^2, $M_X > 2$ GeV and $y < 0.6$. The predictions of the QCD fit for the region $Q_0^2 < Q^2 < Q^2_{\rm cut}$ between the starting scale $Q_0^2 = 3$ GeV^2 for QCD evolution and the minimum Q^2 of data included in the fit $Q^2_{\rm cut} = 6.5$ GeV^2 is shown by the dashed line.

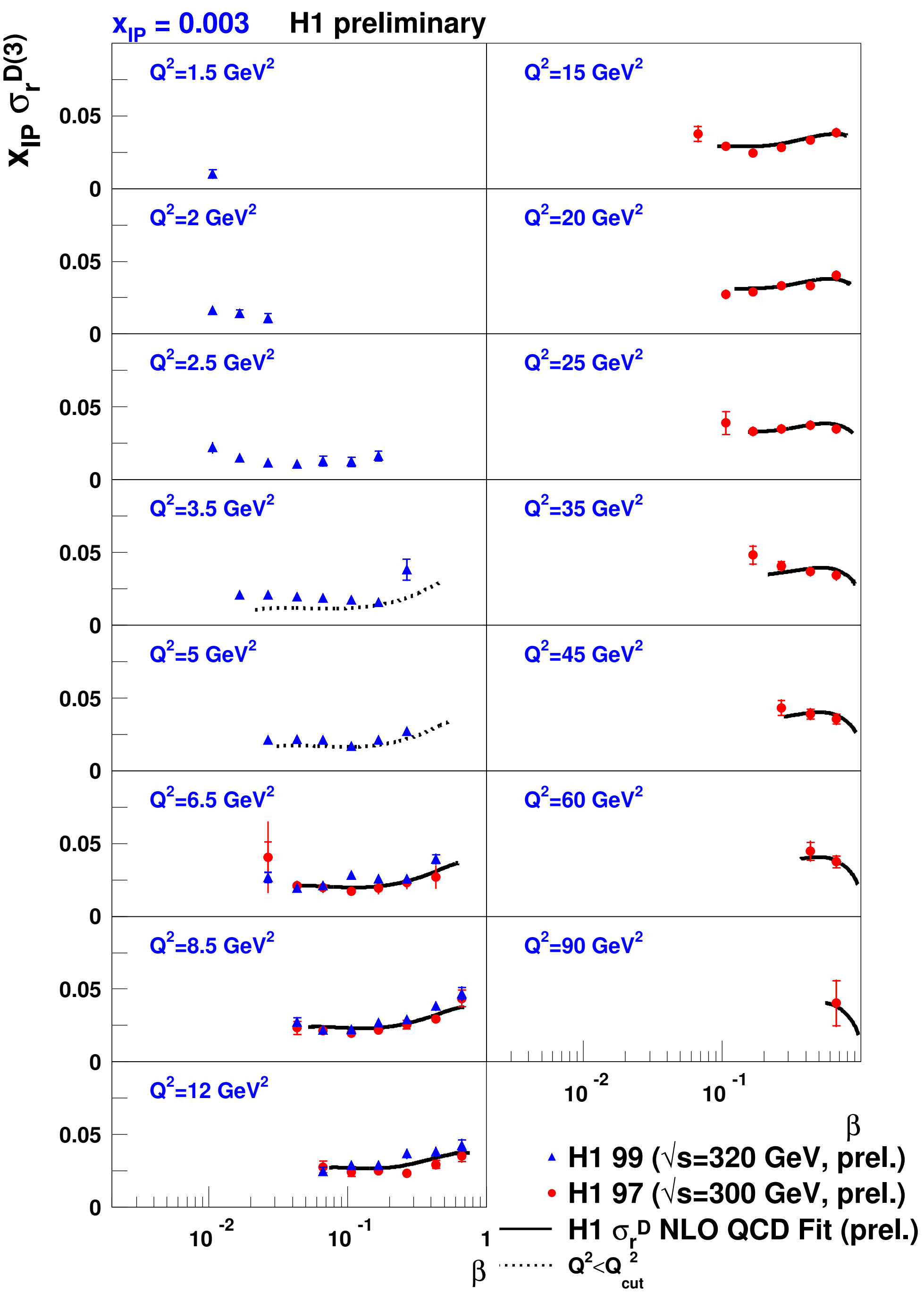

Figure 10: The reduced diffractive cross section $x_{I\!P}\sigma_r^{D(3)}(\beta, Q^2, x_{I\!P})$ (blue triangles) compared with a recent H1 measurement [1] (red circles). $x_{I\!P}\sigma_r^{D(3)}(\beta, Q^2, x_{I\!P})$ is shown as a function of β at $x_{I\!P} = 0.003$ for fixed values of Q^2. The prediction for $x_{I\!P}\sigma_r^{D(3)}$ for $\sqrt{s} = 300$ GeV from the NLO DGLAP QCD fit in [1] is shown with the solid line for $Q^2 \geq 6.5$ GeV^2, $M_X > 2$ GeV and $y < 0.6$. The predictions of the QCD fit for the region $Q_0^2 < Q^2 < Q^2_{\rm cut}$ between the starting scale $Q_0^2 = 3$ GeV^2 for QCD evolution and the minimum Q^2 of data included in the fit $Q^2_{\rm cut} = 6.5$ GeV^2 is shown by the dashed line.

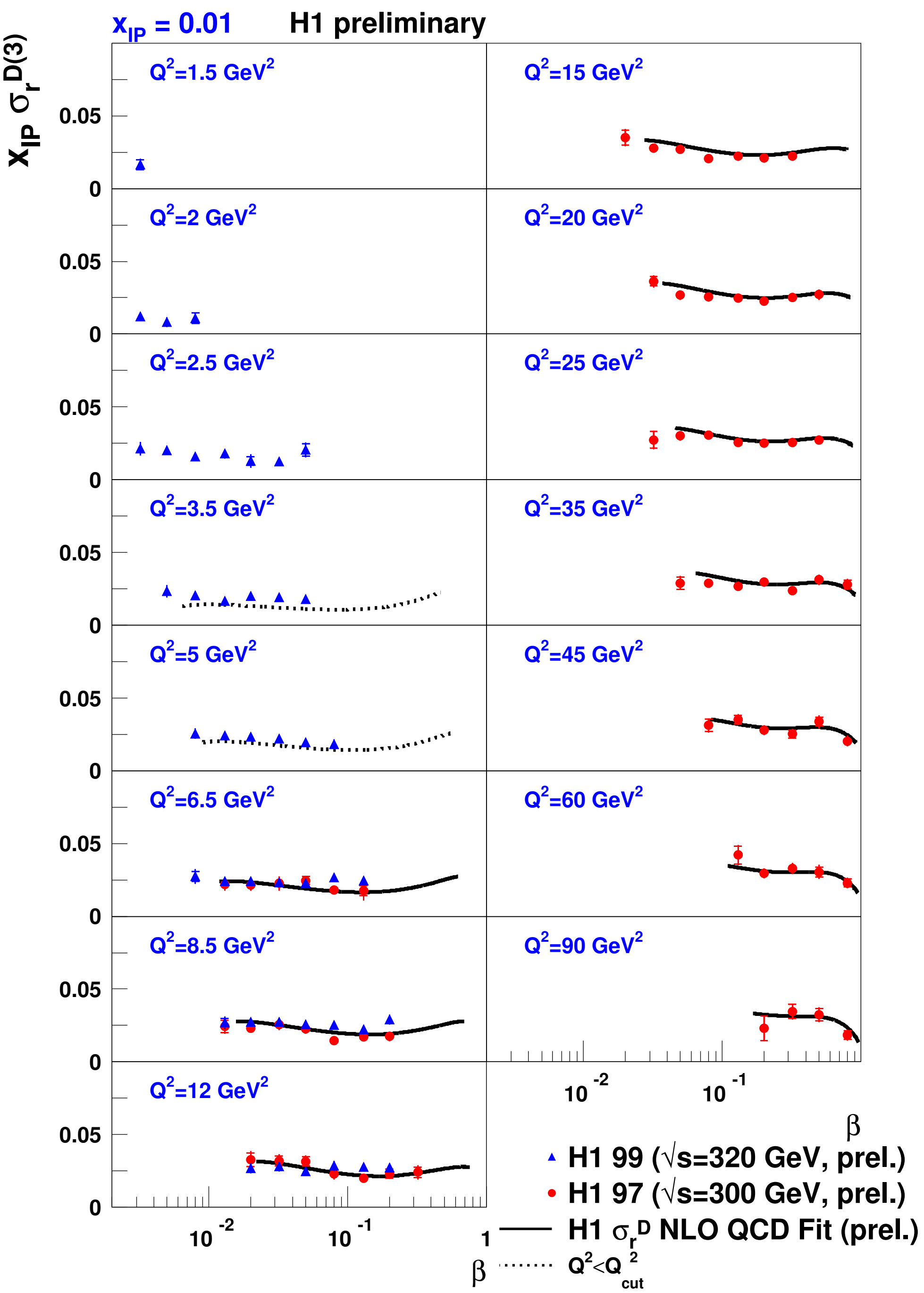

Figure 11: The reduced diffractive cross section $x_{I\!P}\sigma_r^{D(3)}(\beta, Q^2, x_{I\!P})$ (blue triangles) compared with a recent H1 measurement [1] (red circles). $x_{I\!P}\sigma_r^{D(3)}(\beta, Q^2, x_{I\!P})$ is shown as a function of β at $x_{I\!P} = 0.01$ for fixed values of Q^2. The prediction for $x_{I\!P}\sigma_r^{D(3)}$ for $\sqrt{s} = 300$ GeV from the NLO DGLAP QCD fit in [1] is shown with the solid line for $Q^2 \geq 6.5$ GeV^2, $M_X > 2$ GeV and $y < 0.6$. The predictions of the QCD fit for the region $Q_0^2 < Q^2 < Q^2_{\rm cut}$ between the starting scale $Q_0^2 = 3$ GeV^2 for QCD evolution and the minimum Q^2 of data included in the fit $Q^2_{\rm cut} = 6.5$ GeV^2 is shown by the dashed line.

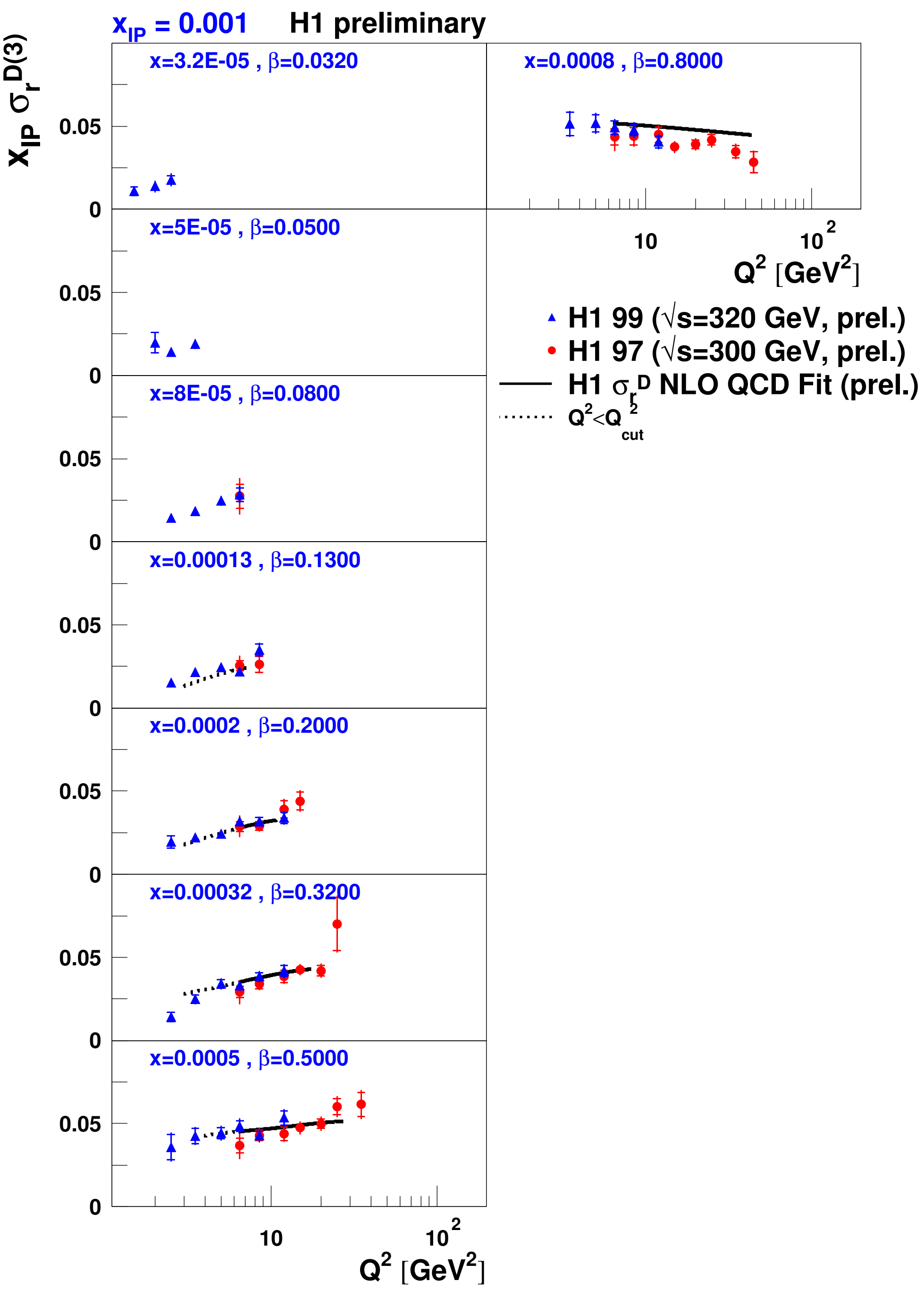

Figure 12: The reduced diffractive cross section $x_{I\!P}\sigma_r^{D(3)}(\beta, Q^2, x_{I\!P})$ (blue triangles) compared with a recent H1 measurement [1] (red circles). $x_{I\!P}\sigma_r^{D(3)}(\beta, Q^2, x_{I\!P})$ is shown as a function of Q^2 at $x_{I\!P} = 0.001$ for fixed values of x and β. The prediction for $x_{I\!P}\sigma_r^{D(3)}$ for $\sqrt{s} = 300$ GeV from the NLO DGLAP QCD fit in [1] is shown with the solid line for $Q^2 \geq 6.5$ GeV^2, $M_X > 2$ GeV and $y < 0.6$. The predictions of the QCD fit for the region $Q_0^2 < Q^2 < Q^2_{\rm cut}$ between the starting scale $Q_0^2 = 3$ GeV^2 for QCD evolution and the minimum Q^2 of data included in the fit $Q^2_{\rm cut} = 6.5$ GeV^2 is shown by the dashed line.

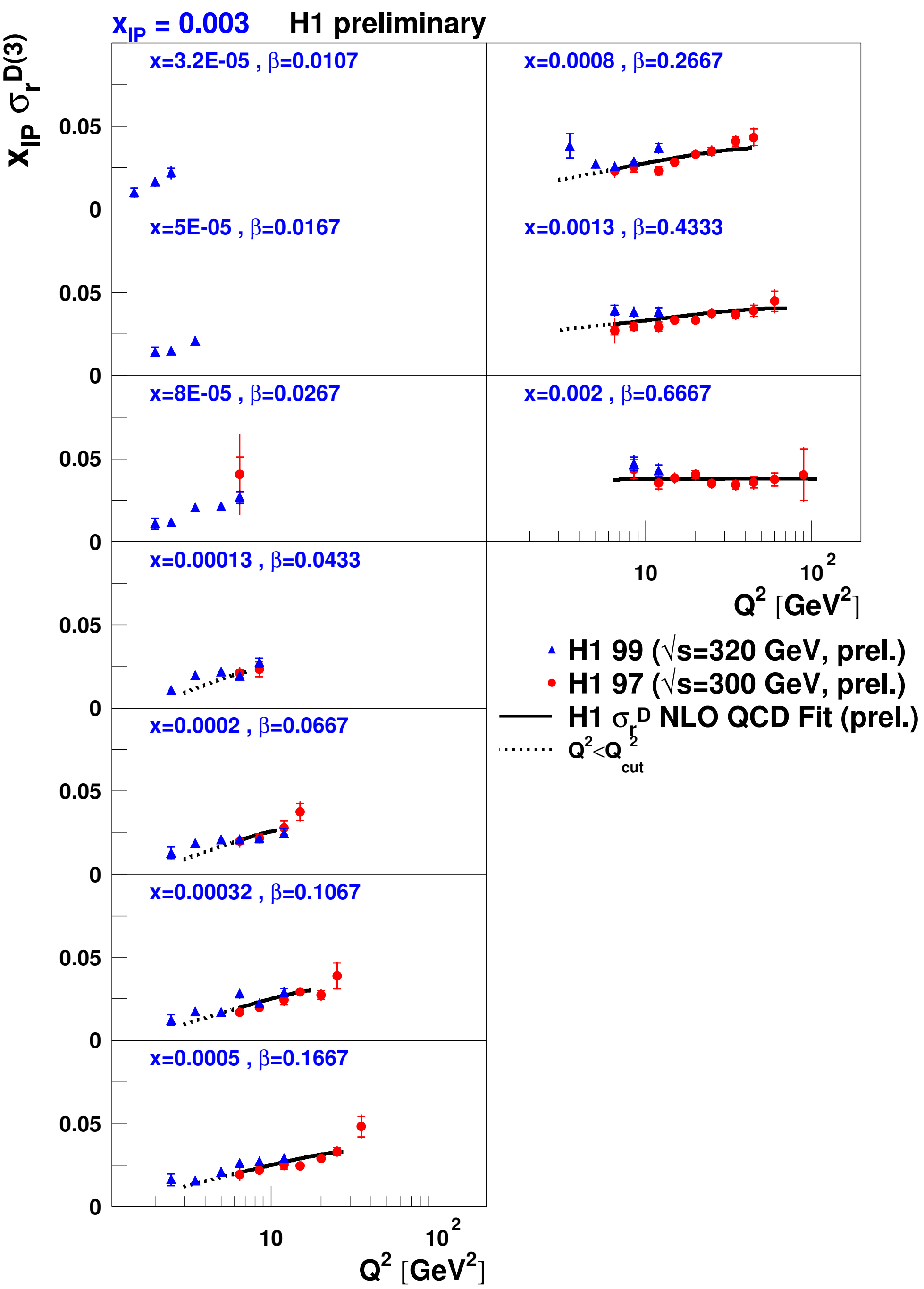

Figure 13: The reduced diffractive cross section $x_{\mathbb{P}}\sigma_r^{D(3)}(\beta, Q^2, x_{\mathbb{P}})$ (blue triangles) compared with a recent H1 measurement [1] (red circles). $x_{\mathbb{P}}\sigma_r^{D(3)}(\beta, Q^2, x_{\mathbb{P}})$ is shown as a function of Q^2 at $x_{\mathbb{P}} = 0.003$ for fixed values of x and β. The prediction for $x_{\mathbb{P}}\sigma_r^{D(3)}$ for $\sqrt{s} = 300$ GeV from the NLO DGLAP QCD fit in [1] is shown with the solid line for $Q^2 \geq 6.5$ GeV^2, $M_X >$ 2 GeV and $y < 0.6$. The predictions of the QCD fit for the region $Q_0^2 < Q^2 < Q^2_{\rm cut}$ between the starting scale $Q_0^2 = 3$ GeV^2 for QCD evolution and the minimum Q^2 of data included in the fit $Q^2_{\rm cut} = 6.5$ GeV^2 is shown by the dashed line.

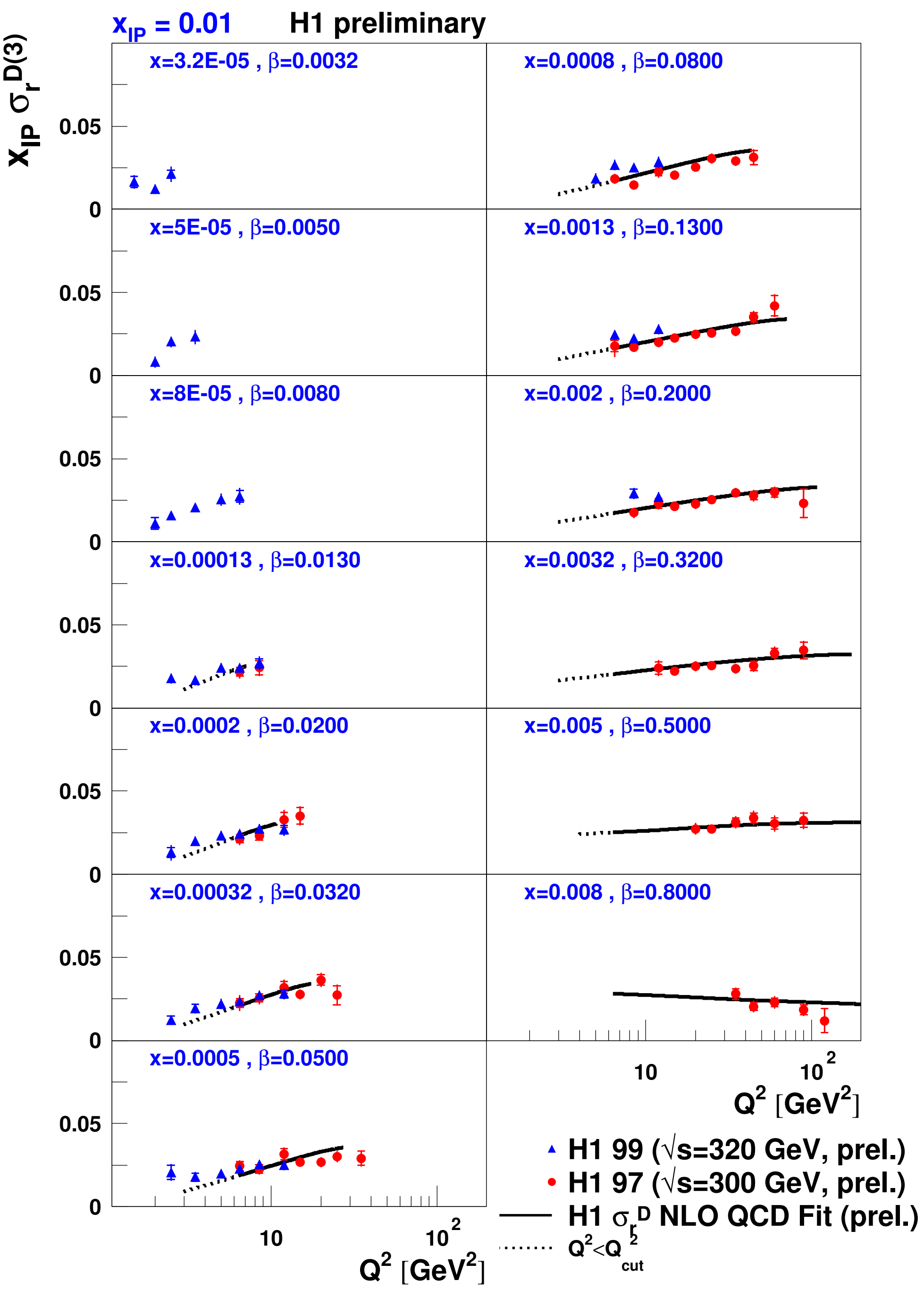

Figure 14: The reduced diffractive cross section $x_{\mathbb{P}}\sigma_r^{D(3)}(\beta, Q^2, x_{\mathbb{P}})$ (blue triangles) compared with a recent H1 measurement [1] (red circles). $x_{\mathbb{P}}\sigma_r^{D(3)}(\beta, Q^2, x_{\mathbb{P}})$ is shown as a function of Q^2 at $x_{\mathbb{P}} = 0.01$ for fixed values of x and β. The prediction for $x_{\mathbb{P}}\sigma_r^{D(3)}$ for $\sqrt{s} = 300$ GeV from the NLO DGLAP QCD fit in [1] is shown with the solid line for $Q^2 \geq 6.5$ GeV^2, $M_X >$ 2 GeV and $y < 0.6$. The predictions of the QCD fit for the region $Q_0^2 < Q^2 < Q^2_{\rm cut}$ between the starting scale $Q_0^2 = 3$ GeV^2 for QCD evolution and the minimum Q^2 of data included in the fit $Q^2_{\rm cut} = 6.5$ GeV^2 is shown by the dashed line.

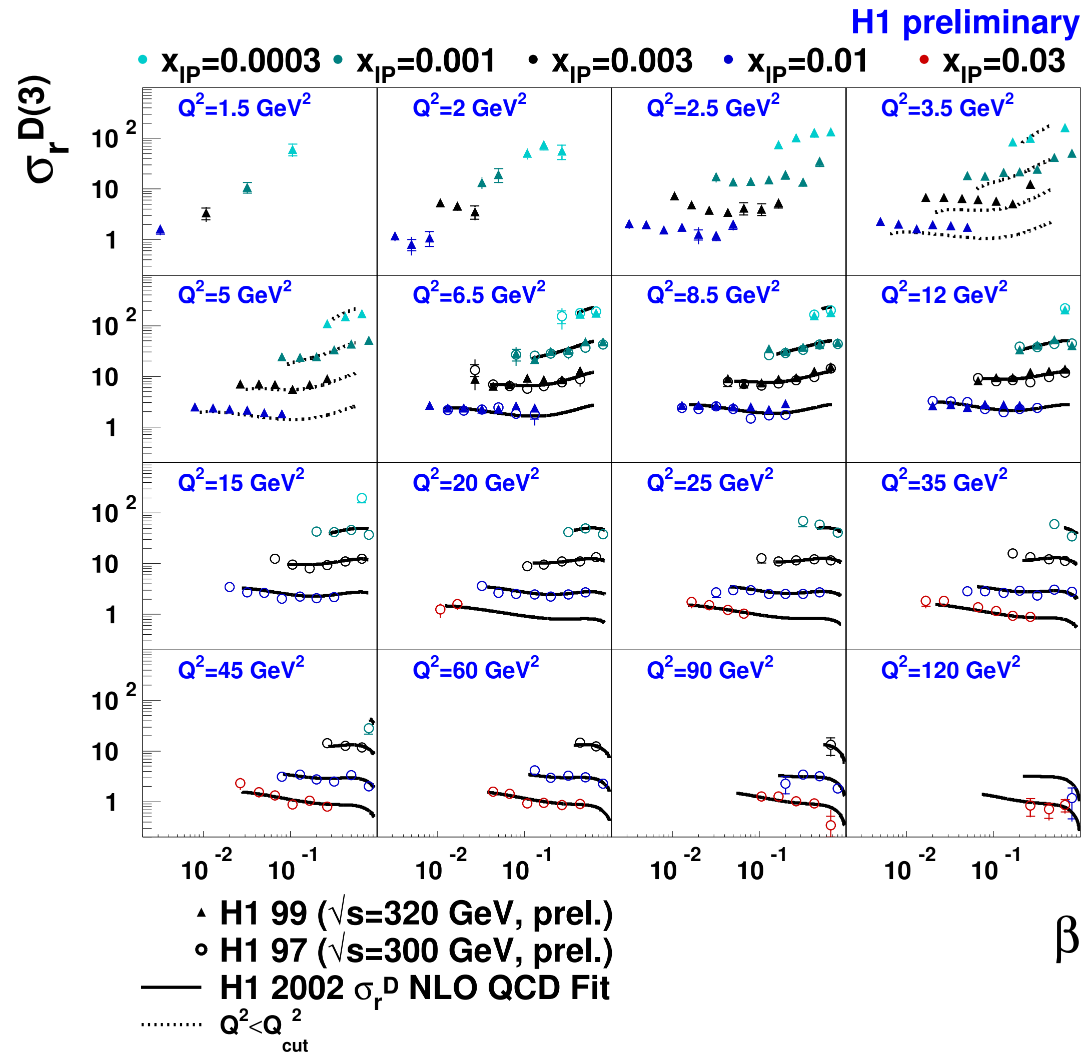

Figure 15: β dependence of the reduced diffractive cross section $\sigma_r^{D(3)}(\beta, Q^2, x_{I\!P})$ from the 1999 (triangles) and 1997 [1] (circles) data. The data are shown at fixed values of Q^2 for $x_{I\!P}$ =0.0003, 0.001, 0.003, 0.01 and 0.03. The prediction for $x_{I\!P}\sigma_r^{D(3)}$ for $\sqrt{s} = 300$ GeV from the NLO DGLAP QCD fit in [1] is shown with the solid line for $Q^2 \geq 6.5\ \mathrm{GeV}^2$, $M_X > 2$ GeV and $y < 0.6$. The predictions of the QCD fit for the region $Q_0^2 < Q^2 < Q^2_{\mathrm{cut}}$ between the starting scale $Q_0^2 = 3\ \mathrm{GeV}^2$ for QCD evolution and the minimum Q^2 of data included in the fit $Q^2_{\mathrm{cut}} = 6.5\ \mathrm{GeV}^2$ is shown by the dashed line.

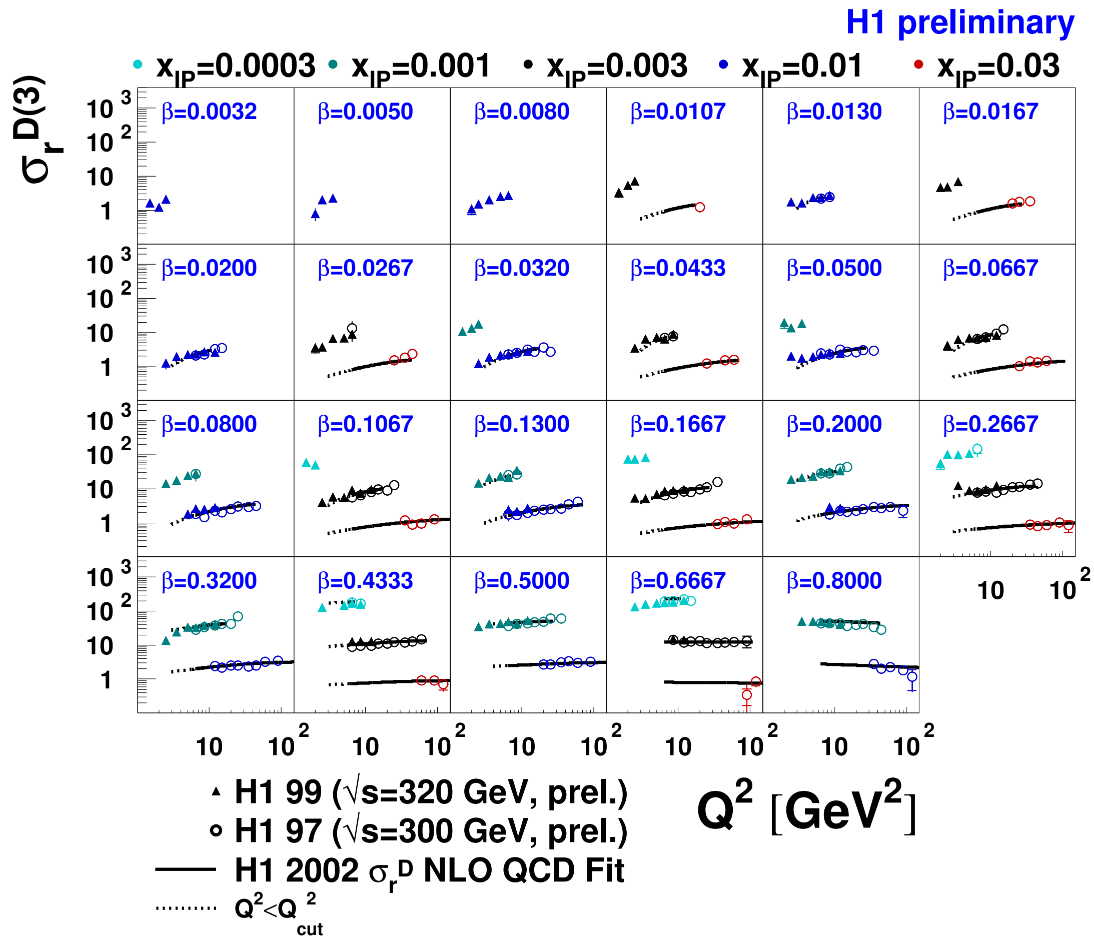

Figure 16: Q^2 dependence of the reduced diffractive cross section $\sigma_r^{D(3)}(\beta, Q^2, x_{I\!P})$ from the 1999 (triangles) and 1997 [1] (circles) data. The data are shown at fixed values of β for $x_{I\!P}$ =0.0003, 0.001, 0.003, 0.01 and 0.03 simultaneously. The prediction for $x_{I\!P}\sigma_r^{D(3)}$ for $\sqrt{s}$ = 300 GeV from the NLO DGLAP QCD fit in [1] is shown with the solid line for $Q^2 \geq 6.5$ GeV^2, $M_X > 2$ GeV and $y < 0.6$. The predictions of the QCD fit for the region $Q_0^2 < Q^2 < Q^2_{\rm cut}$ between the starting scale $Q_0^2 = 3$ GeV^2 for QCD evolution and the minimum Q^2 of data included in the fit $Q^2_{\rm cut} = 6.5$ GeV^2 is shown by the dashed line.

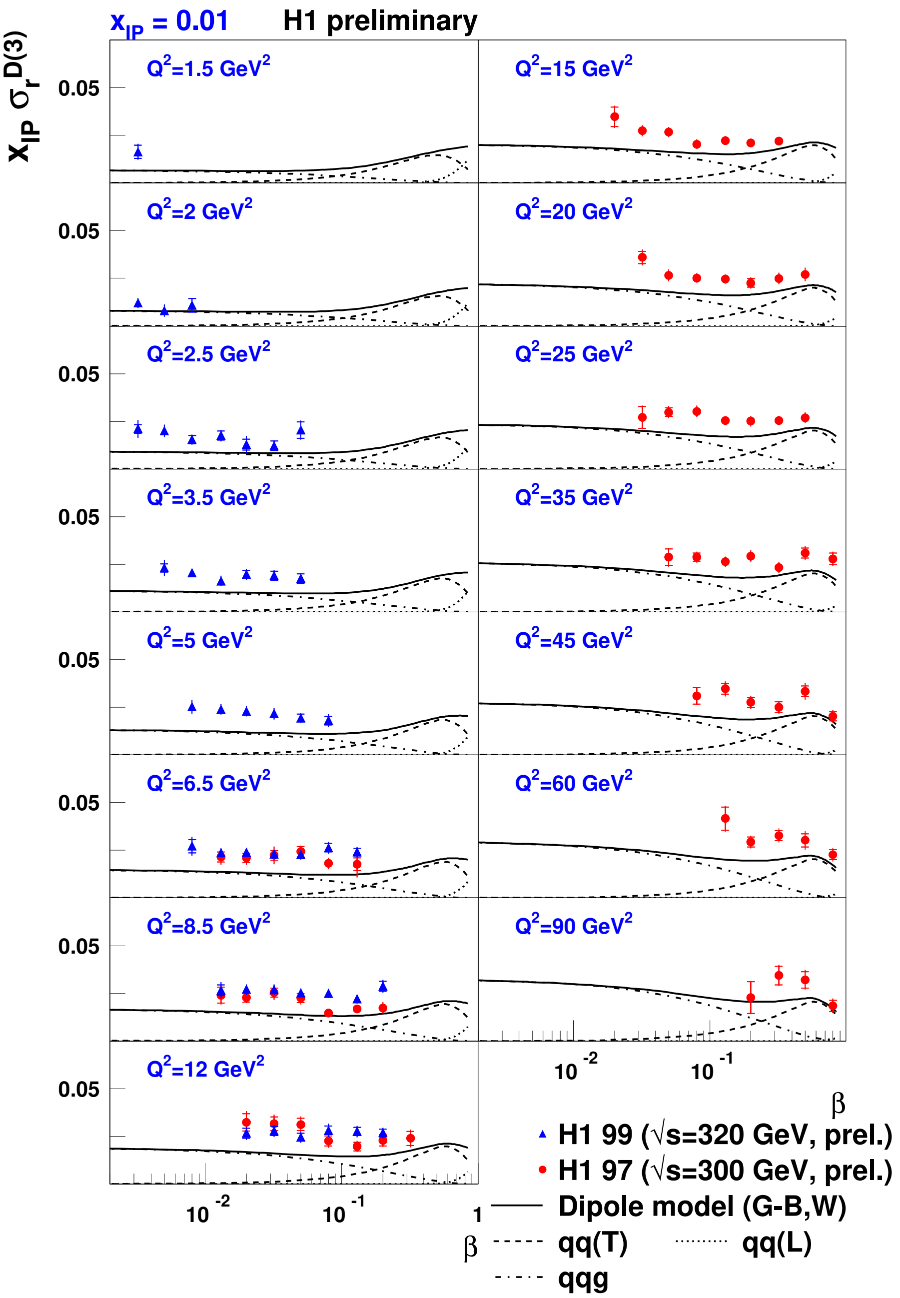

Figure 17: The diffractive reduced cross section $x_{I\!P}\sigma_r^{D(3)}(\beta, Q^2, x_{I\!P})$ from the 1999 (triangles) and 1997 [1] (circles) data, shown as a function of β for fixed Q^2 values and $x_{I\!P} = 0.01$. The data are compared with the prediction of the dipole model of Golec-Biernat and Wüsthoff [9, 18], with the exponential slope parameter of the t distribution chosen to be $B = 6$ GeV^{-2}. The contributions in the model from the scattering of $q\bar{q}$ fluctuations of longitudinally polarised photons and $q\bar{q}$ and $q\bar{q}g$ fluctuations of transversely polarised photons are also shown separately.